Mardali, M.; Salimijazi, H.; Karimzadeh, F.; Luthringer-Feyerabend, B.J.C.; Blawert, C.; Labbaf, S.:
Fabrication and characterization of nanostructured hydroxyapatite coating on Mg-based alloy by high-velocity oxygen fuel spraying.
In: Ceramics International. Vol. 44 , , (2018) 12, 14667 - 14676.
First published online by Elsevier: May 26, 2018

DOI: /10.1016/j.ceramint.2018.05.093
https://dx.doi.org/10.1016/j.ceramint.2018.05.093

Fabrication and characterization of nanostructured hydroxyapatite coating on Mg-based alloy by High-velocity oxygen fuel spraying

Marzieh Mardali[a,b*], Hamidreza Salimijazi[a], Fathallah Karimzadeh[a], Berengere J. C. Luthringer-Feyerabend[b], Carsten Blawert[c], Sheyda Labbaf[a]

[a] Department of Materials Engineering, Isfahan University of Technology, Isfahan 84156-83111, Iran

[b] Institute of Materials Research, Division of Metallic Biomaterials, Helmholtz-Zentrum Geesthacht, 21502 Geesthacht, Germany

[c] Magnesium Innovation Centre, Institute of Materials Research, Helmholtz-Zentrum Geesthacht, 21502 Geesthacht, Germany

Abstract

Magnesium alloys are currently being investigated in orthopedic applications due to their biodegradability and mechanical properties. However, sometimes these benefits are limited by their high corrosion rate in the physiological environment before healing of damaged bones. A large number of recent researches in this field have been dedicated to the control of magnesium corrosion rate by surface protection using new and advanced coatings. In this work, hydroxyapatite powders were coated on the anodized Mg-based alloy substrates by using high velocity oxy-fuel (HVOF) spraying. Increasing of the bioactivity and reduction of the released hydrogen gas during corrosion of the substrate were two main objects of this work. Phase formations were characterized by X-ray diffraction (XRD). It was found that around 96% of the phases formed were hydroxyapatite. The amounts of hydrogen gas released during magnesium corrosion tests in the simulated body fluid (SBF) were measured to evaluate the corrosion resistance of the coated samples. Hydroxyapatite (HA) coating reduced the hydrogen evolution from 100 per cm^2.mL to about 15 per cm^2.mL after 29 hours of immersion.

Keywords: High Velocity Oxygen Fuel spraying, Corrosion, Apatite, Biomedical application

*Corresponding author

Email address: Marzie.mardali@gmail.com

1. Introduction

Hydroxyapatite (HA) coatings are widely used for a range of biomedical applications, in particular orthopedic, dental and maxillofacial. HA coatings have the ability to shorten the healing process of metal implants since they are bioactive, osteoconductive and osteoinductive and also enhance osseointegration and bone growth *in vivo* [1]. HA is chemically similar to the mineral phase of bone and it is therefore an ideal candidate for biomedical coating applications [2, 3].

Combination of high strength and flexibility of magnesium make it to be more attractive than ceramic and polymer biodegradable materials. Magnesium is essential to human metabolism, and its elastic modulus is matched to the natural bone which can reduce stress shielding effect. However, these alloys have some disadvantages including high corrosion rate and release of hydrogen gas as a reaction product during corrosion [4-8].

Today, extensive researches are underway to solve the problem of high corrosion rate of magnesium. For this purpose, either the chemical composition of the alloy must be engineered [9, 10] or a protective layer of coating must be deposited on the surface [11]. Lack of sufficient strength and limitations in choosing biocompatible alloying elements limits the modification of the chemical composition of the alloy [12]. Several coating techniques such as sol-gel [13-15], bio-mimetic coating [16, 17], thermal spraying [18], electrochemical deposition [19, 20], anodizing [21, 22], RF sputtering [23], chemical vapor deposition (CVD) and physical vapor deposition (PVD) [24] have previously been employed. Amongst various

coating methods, plasma spray technique is one of the approved method by US Food and Drug Administration (FDA) for implants coating [25].

HVOF spray principle is based on combustion of fuel and oxygen gases in a chamber. This technique is fast and affordable for large-scale production, and it does not require any post-deposition heat treatment like electrophoretic deposition technique. HVOF uses a low temperature flame. Therefore, fewer phase transformations took place in particular for HA coatings [27]. Another benefit of HVOF method is the high pressure of the gas stream during coating. This creates more adhesion strength of coating to the substrate and less porosity and therefore, less corrosion rate. Also, the ability to create nano structured coatings in the case of using nano structured feed stock powders can be an advantage. Moreover, it shows higher density and less porosity than other thermal spraying methods. This technique has been used already for coating of HA on titanium and stainless steel implants [28]. However, there are limited studies on HA coating on magnesium alloys for biomedical applications by using HVOF spraying [29-31].

In this study, nano structured hydroxyapatite powders were coated on magnesium alloy (AZ61) by HVOF method. Anodized coating was used for reduction of the thermal expansion coefficient difference between the magnesium substrate and hydroxyapatite layer, and therefore decreasing the residual stresses in the coating. On the other hand, it can increase the corrosion resistance of the Mg substrate. The main objective of this research was to investigate the relationship between the microstructure and phase composition of the HA coating deposited by HVOF and the amount of the released hydrogen in the SBF solution during corrosion.

2. Materials and methods

2.1. Samples preparation and coatings

Initial HA powders were produced by degreasing of the crashed bovine bone. To remove black parts including carbonic products, calcination at 1200 °C for 2 h was conducted. In order to achieve nano structured powders, bone pieces were milled by high-energy planetary milling (Retsch, PM100) with a rotational speed of 250 rpm and a ball to powder ratio of 10:1 for 8 h. For modification of the morphology of the obtained particles to achieve a more spherical particle shape, they were dried by spray drying (LabPlant SD-basic spryer dryer). The solution was distilled water at 0.05 mol/lit concentration of suspension, pump flow 5 bar and inlet temperature was 115 °C.

AZ61B-H24 wrought alloy (mass fraction: Al 5.50%, Zn 1.5%, Mn 0.78%, Si<0.02%, balance Mg) was used as the substrate. Sand blasted (Aluminum oxide, 30 mesh) specimens sized 15×15×5 mm were degreased in NaOH (10 g in 100 ml water) at 70 ˚C for 5 min as a cleaning process. The anodizing was carried out in 3 M KOH and 1.3 M $Na_3(PO_4)$ at 25 ˚C using a DC power supply (IPC-SL20200J, Iran). The distance between the two electrodes was 4 cm. The cathode was a plate of stainless steel (25×30×3 mm), and samples were anodized under constant voltage of 70 V for 60 min. Small sparks were observed continuously on the surface of the sample.

Thermal spraying of the feedstock was performed by using HVOF spray system (K2-GTV, Germany) torch. The parameters of the HVOF spray are shown in Table 1.

2.2. Characterization

The phase composition of coatings was studied using X-ray diffraction (XRD) (Bruker D8) with Ni filtered CuKalpha ($\lambda_{CuK\alpha}$ = 1.54056 Å, radiation at 40 KV and 30 mA) and with a step size of 0.05 ° and a count time of 1.25 s per step.

Crystallite size of the coatings was measured using the modified Scherrer formula (Eq. 1) [32]:

$$\ln\beta = \ln\frac{0.9\lambda}{D} + \ln\frac{1}{\cos\theta} \quad (1)$$

Where β (rad) is full-width half maximum of peaks (FWHM), θ (°) is the diffraction angle, λ=0.154056 (nm) is the wavelength of the X-ray, D (nm) is the grain size. For this purpose, some diffraction peaks which have high intensities that they are attributed to HA phase were selected. In addition to the sample, diffractometer also makes peaks broadening that it is called $\beta_{instrument}$. To measure this parameter, quartz (SiO_2) was used as standard. Quantitative measurements of phase composition were performed using Rietveld refinements method and the structural models of American Mineralogist crystal Structure (AMS) database reference files for calcium phosphate, Mg and MgO phases. Maud software with the fundamental parameters approach was employed. Scale factor, specimen displacement, and background as Chebyshev polynomial of fifth grade and 1/x function, crystallite size, micro-strain, and lattice parameters were refined parameters [32].

The powder particles morphology before and after spray drying, surface topography and cross-sections of the coatings were examined using SEM and field emission scanning

electron microscopy (FE-SEM). Additionally, samples were broken in liquid nitrogen and morphology of the fractured surfaces was characterized by SEM.

Elemental distribution map of HA coatings was characterized by EDS analyzer. To investigate the hydrogen evolution reaction on the coated samples, immersion tests in SBF solution ware performed in a eudiometer. The composition of the SBF solution which is used for hydrogen evolution test is given in Table 2. To protect other sides of the sample from corrosion, they were masked with resin (Methyl methacrylate).

Optical micrographs from the cross sections of the coatings were taken to study the magnesium alloy stability in the HVOF process. A solution of acetic acid 7 ml, distilled water 35 ml, ethanol 140 ml and picric acid 6-7 g was used as etchant agent. Grain size measurements were carried out according to the Heyn intercepts method-ASTM E112.

3. Results

3.1. Powders characterization

Fig 1 (a) shows the morphology of natural hydroxyapatite powders derived from bovine bone before spray drying process with uniform particle size distribution. Particles were generally adhered to each other, and therefore, they do not have sufficient flowability. The particle size was in the range of 0.5 to 0.9 μm and their morphology was semi-spherical. Fig 1 (b-c) present the morphology of the powders after spray drying. The formation of the semi-spherical agglomerated particles in the range of 17 to 20.5 μm in size would enhance the flowability of the powders. Fig 2 shows the XRD pattern of HA powders after spray drying.

The main phase composition of powders was HA (94% HA and 6% CaO). The crystallite size of the synthesized powders was around 34 nm. It was measured by Eq.1.

3.2. Development of MgO intermediate layers

Fig 3(a) shows the surface morphology of the MgO coating deposited by anodizing process. This layer was not dense and some homogenously distributed pores were presented within the surface of the coating. Some large cavities were created as a result of big sparks formation during anodizing [33]. Pores diameters were in the range of 0.3 to 1.1 μm. The cross-section morphology of this layer is demonstrated in Fig 3(b). The thickness of the anodized layer was between 10 to 13.2 μm. Fig 3c shows the fracture surface of the sample in liquid nitrogen. The XRD pattern of the anodized layer confirms the formation of MgO phase on the Mg alloy surface (Fig 4).

3.3. Characterization of the surface of the coated samples

The phase composition of HA coatings are shown in Fig 5. The XRD patterns show that peaks are clearly sharp indicating high degree of crystallinity which can be due to the nature of the deposition by HVOF. The majority of the formed phase was HA (96%), but Mg (2%), α-TCP (Tri Calcium Phosphate) (1%) and MgO (0.5%) were also observed. The crystallite size calculated from Eq. 1 was around 36 nm.

The thickness of the sprayed layer was in the range of 11.9 to 29 μm (Fig 6). It appears that after HVOF deposition, the thickness of the MgO layer decreased from around 11.6 to 2.8 μm. In fact, HVOF acts as a blasting process.

Surface morphology of the coating is shown in Fig 7. It is dominated by flattened splats and partially or semi-melted and small amount of un-melted particles. High velocity of feedstock during spraying makes incomplete spreading of splats. Particles still remain in their spherical shape. The surface is rough in result of this incomplete spreading and un-melted particles. Fig 8 shows some un-melted and partially molten particles on the surface of HA coatings. Agglomerated essence of the feedstock remained in the coagulation of semi-molten particles or sintered un-melted particles in the surface of HA lamella.

Elemental linear analysis can be seen in Fig 9. The amount of magnesium increased from left to the right. The elemental distribution by mapping is shown in Fig 10. There was no magnesium throughout the surface. Therefore, magnesium was stable during HVOF spraying. This analysis also shows the uniformity of the chemical composition in the coating. The calculated Ca/P ratio from Table 3 was found to be 1.7.

3.4. Thermal stability of magnesium alloy

The microstructures of the substrate near (a) and 2 mm away (b) from the coating/substrate interface are shown in Fig 11. Crystallographic stability of the Mg alloy substrate can be seen in Fig 11 (a). There was no trace of amorphous phase dissolution in the etchant even near the sub surface. Grain growth in the near surface areas is obvious. This can be due to the exposure of the substrate surface to high-temperature during HVOF spraying. The size of grains can influence the corrosion rate of the Mg substrate. By increasing the grain size, the grain boundaries densities are reduced in the near surface regions, which could increase the corrosion resistance of the alloy [34]. Grain size for near the surface region was between 8

to 36 μm and for the area away from the surface of the substrate was in the range of 5 to 11 μm.

3.5. Hydrogen evolution test

The amount of hydrogen gas released during magnesium corrosion in the SBF solution for up to 30 h immersion is shown in Fig 12. A significant difference between uncoated and anodized and hydroxyapatite coated samples can be observed in the early stage of immersion. Both anodized and anodized plus HA coated samples exhibited relative uniform corrosion behavior for up to 10 h. But after that, the amount of the released hydrogen from the anodized samples was much higher than that for the anodized and HA coated samples. Therefore, it could be concluded that the secondary HA coating also had barrier effect on the corrosion resistance of the Mg alloy. Furthermore, the measured pH of SBF after 30 immersion for the bare alloy, anodized and anodized plus HA coated were 8.5, 7.8 and 7.6, respectively.

Fig 13 shows surfaces of Mg-alloy, anodized, and anodized plus HA coated samples after 29 h of immersion. The observations verified the results from H_2 release. The white particles were found on the surface of all samples. In Table 4 it is found that the corrosion rate is higher in the case of non-coated magnesium alloy samples than the rest of samples.

In Fig 14, morphology and analysis of the surface of the anodized and HA coated sample after hydrogen evolution test is shown. Table 5 demonstrated results of EDS for the corroded surfaces. The ratio of Ca/P was increased after immersion of samples in SBF. This is an indication of the deposition of Ca^{2+} and HPO_4^{2-} ions after immersion [35].

4. Discussion

4.1. MgO bond coat

It is expected from this layer that, in addition to protect the substrate from corrosion, it reduces the gradient of thermal expansion coefficient (TEC) between the secondary coating (hydroxyapatite) and the magnesium alloy substrate. Thermal expansion coefficient of magnesium alloy, HA and MgO are about $26.0\times10^{-6}\ °K^{-1}$, $14\times10^{-6}\ °K^{-1}$ and $13.8\times10^{-6}\ °K^{-1}$, respectively. Therefore, by reducing the TEC gradient between the hydroxyapatite coating and the magnesium oxide layer, it is expected to see a lower residual stress in the HA coating. In addition, the anodized layer can act as a corrosion protection layer. So, it prevents superficial cracks during HVOF spraying [36].

4.2. Thermal decomposition of HA coating

It is well known that dissolution rate of various calcium phosphate phases in the physiological environment follows HA<TCP<TTCP (tetra calcium phosphate) <ACP (amorphous calcium phosphate) [25]. According to $CaO\text{-}P_2O_5$ phase diagram, HA is decomposed to form a mixture of $\alpha'\text{-}Ca_3(PO_4)_2$ and $Ca_4O(PO_4)_2$ with the loss of a water molecule. Also, the amorphous phase is preferentially forming due to: 1) quenching of the melt 2) lack of enough time to form a complex hexagonal structure and 3) insufficient structural water [25]. So, the percentage of these unstable phases can influence the degradability of the final product. Therefore, the degree of solubility of this coating, on the one hand, affects the corrosion rate of the entire product and hence is affecting the surface bioactivity.

In this work, the temperature and pressure applied to HA particles during HVOF technique is not enough to melt the particles completely. Therefore, the amount of intermediate phases in the final product is less in comparison to other thermal spray methods.

4.3. Microstructural study

Some intersplat cracks in the coating can be observed in Fig 6 which could be due to the nature of the thermal spray coating of ceramic materials. Moreover, the formation of vertical and horizental cracks could be related to the gradient of thermal expansion coafficient between HA and Mg substrate. Although the presence of an intermediate layer of magnesium oxide has reduced this gradient, but this effect has diminished due to reduction of its thickness during the spray process. On the other hand, It can not be denied the development of cracks as a result of cross-sectional sample preparation. Rough surface at the coating/substrate interface can be attributed to the preparation of the substrate by sand blasting before anodizing. Anodizing can also roughen the interface by creating pores.

The existence of nanostructured agglomerates on the surface of the coating makes desirable active surfaces for the cultivation of pseudo bone like apatite after placement in the physiological fluid. It is known that nano-structured coating increase the effective surface area and sites for nucleation of apatite crystals and as a result, increase of the tendency of stronger bone bonding and cell attachment and growth take place [37].

In Fig 9, curves can be divided into three regions, calcium phosphate layer, anodized layer and the magnesium alloy substrate with the highest amount of magnesium and lack of calcium, phosphorous and oxygen. Fluctuations in the part of calcium phosphate layer could

be due to the inter-splat cracks in the coating. It was observed that as the depth of coating was reduced toward the substrate, the relative amount of calcium and phosphorus increased by reduction of oxygen content. It can be explained that less feedstock were placed on the upper layers of the coating. As a result, the cooling rates of these layers splats will be higher during spray. More roughness of the mentioned interface compared to upper layers may make lower thermal conductivity. Therefore, in the surface layers, the amount of oxy-apatite phases with lower oxygen content was higher. The presence of more stable phases in the interface has beneficial to guarantee durable bond strength.

4.4. Corrosion products

Magnesium corrosion mechanism can be describe by the following equations [8]:

Anodic reaction

$$Mg + H_2O \rightarrow Mg^{2+} + OH^- + 1/2H_2 + e^- \quad (3)$$

Cathodic reaction

$$Mg + 2H_2O \rightarrow Mg(OH)_2 + H2\uparrow \quad (4)$$

The dissolution of magnesium was accompanied by the hydrogen evolution reaction that was responsible for increasing the pH of SBF solution. One of the best methods to anticipate magnesium corrosion is the hydrogen evolution test [13]. By this approach, it is demonstrated that the corrosion resistance of untreated samples was significantly increased by anodizing and HVOF process. The pH of the SBF solution increases as the result of OH^- ion formation during corrosion. More pH indicates more corrosion rate [31].

HA coating facilitated the precipitation of white particles on the surface compared to the AZ61 and anodized samples. These particles are likely to be precipitates of calcium phosphate after immersion in the SBF solution. The alkaline environment caused by magnesium corrosion is effective in supporting the formation of these white precipitates, by deposition of Ca^{2+} and HPO_4^{2-} ions onto the surface.

5. Conclusions

HVOF method is shown to be a capable way to coat magnesium alloy AZ61 with hydroxyapatite powders. In this work, by applying magnesium oxide and hydroxyapatite coatings, the amount of hydrogen released by the corrosion of the magnesium alloy substrate decreased, especially in the early stages of corrosion. Hydrogen evolution rate decreased after anodizing and deposition of HA from 45.8 per cm^2.mL to about 7.38 per cm^2.mL after 29 h of immersion. The high amount of the stable phase of the HA in the coating is also due to its low thermal decomposition during coating at relatively low temperature of spraying technique. Magnesium alloy substrate tolerated both the high temperature and high speed of particles during HVOF coating. Also, the coating had good coverage of Mg alloy substrate and the elements were distributed uniformly. Moreover, nano structured HA was successfully deposited which can improve bio-mimetic surface by creating active sites. It was also found that the amount of calcium phosphate deposited on the surface, was higher in the HA coated sample than others. As a result, the presence of hydroxyapatite coating contributes to the formation of this protective layer.

Our future research will be focused on the optimization of HVOF technical parameters so that the anodized layer shows the least damage.

Acknowledgements

The financial support received from Isfahan University of Technology of Iran and Helmholtz Zentrum Geesthacht of Germany is acknowledged.

References

[1] S.T. Aruna, S. Kulkarni, M. Chakraborty, S. SenthilKumar, N.Balaji, C. Mandal, A comparative study on the synthesis and properties of suspension and solution precursor plasma sprayed hydroxyapatite coatings, Ceram. Int.43 (2017) 9715-9722.

[2] A. H. M. Sanchez, B. J. C. Luthringer, F. Feyerabend, R. Willumeit, Mg and Mg alloys: How comparable are in vitro and in vivo corrosion rates? A review, Acta Biomater. 13 (2015) 16-31.

[3] S. Saber-Samandari, K. Alamara, S. Saber-Samandari, Calcium phosphate coatings: Morphology, micro-structure and mechanical properties, Ceram. Int. 40 (2014) 563-572.

[4] C. Castellani, R. A. Lindtner, P. Hausbrandt, E. Tschegg, S. E. Stanzl-Tschegg, G. Zanoni, S. Beck, A.-M. Weinberg, Bone–implant interface strength and osseointegration: Biodegradable magnesium alloy versus standard titanium control, Acta Biomater. 7 (2011) 432–440.

[5] C.C. Berndt, F. Hasan, U. Tietz, and K. P. Schmitz, A Review of Hydroxyapatite Coatings Manufactured by Thermal Spray, in: B. Ben-Nissan, ED. Berlin, Advances in Calcium Phosphate Biomaterials, Springer Berlin Heidelberg, Heidelberg, 2014, pp. 267-329.

[6] *G-L. Song*, Corrosion Prevention of Magnesium Alloys, Woodhead Publishing, 2013, pp 3-37.

[7] G. Eddy Jai Poinern, S. Brundavanam, D. Fawcett, Biomedical Magnesium Alloys: A Review of Material Properties, Surface Modifications and Potential as a Biodegradable Orthopaedic Implant, Am. J. Biomed. Eng. 2 (2013) 218–240.

[8] S. Virtanen, Biodegradable Mg and Mg alloys: Corrosion and biocompatibility, Mater. Sci. Eng. B Solid-State Mater. Adv. Technol.176 (2011) 1600–1608.

[9] Y. Wang, D. Tie, R. Guan, N. Wang, Y, Shang, T. Cui, J. Li, Microstructures, mechanical properties, and degradation behaviors of heat-treated Mg-Sr alloys as potential biodegradable implant materials, J. Mech. Behav. Biomed. Mater. 77 (2018) 47–57.

[10] Y. Chen, Z. Xu, C. Smith, J. Sankar, Recent advances on the development of magnesium alloys for biodegradable implants, Acta Biomater. 10 (2014) 4561–4573.

[11] M. Dinu, A.Ivanova,M. A.Surmeneva,M. Braic,A..Tyurin,V. Braic et al. Tribological behaviour of RF-magnetron sputter deposited hydroxyapatite coatings in physiological solution, Ceram. Int. 43 (2017) 6858-6867.

[12] M. Esmaily, J.E. Svensson, S. Fajardo, N. Birbilis, G. S. Frankel, S. Virtanen, R. Arrabal, S. Thomas, L. G. Johansson, Fundamentals and advances in magnesium alloy corrosion, Prog. Mater. Sci. 89 (2017) 92–193.

[13] S. Singh, R. Manoj Kumar, K. K. Kuntal, P. Gupta, S. Das, R. Jayaganthan, P. Roy, D. Lahiri, Sol–Gel Derived Hydroxyapat Coating on Mg-3Zn Alloy for Orthopedic Application, JOM. 67 (2015) 702–712.

[14] B. Niu, P. Shi, E. Shanshan, D. Wei, Q. Li, Y. Chen, Preparation and characterization of HA sol–gel coating on MAO coated AZ31 alloy, Surf. Coatings Technol. 286 (2016) 42–48.

[15] C. Domínguez-Trujillo, C. Domínguez-Trujillo, E. Peón, E. Chicardi, H. Pérez, J. A. Rodríguez-Ortiz, J. J. Pavón, J. García-Couce, J. C. Galván, F. García-Moreno, Y. Torres, Sol-gel deposition of hydroxyapatite coatings on porous titanium for biomedical applications, Surf. Coatings Technol. 333 (2018) 158–162.

[16] W. Cui, E. Beniash, E. Gawalt, Z. Xu, C. Sfeir, Biomimetic coating of magnesium alloy for enhanced corrosion resistance and calcium phosphate deposition., Acta Biomater. 9 (2013) 8650–9.

[17] M. B. Kannan, Hydroxyapatite coating on biodegradable magnesium and magnesium-based alloys, in: *M. R. Mucalo,* Hydroxyapatite (HAp) for Biomedical Applications, Woodhead Publishing Series in Biomaterials, 2015, pp. 289–306.

[18] E. SáraBogya,Z. Károly,R. Barabás, Atmospheric plasma sprayed silica–hydroxyapatite coatings on magnesium alloy substrates , Ceram. Int. 41 (2015) 6005-6012.

[19] F. Tjiang, L-W. Ye, Y-J. Huang, C-C. Chou, D-S. Tsai, Effect of processing parameters on soft regime behavior of plasma electrolytic oxidation of magnesium, Ceram. Int. 43 (2017) S567-S572.

[20] R. Rojaee,M. Fathi,K. Raeissi,M. Taherian, Electrophoretic deposition of bioactive glass nanopowders on magnesium based alloy for biomedical applications, Ceram. Int. 40 (2014) 7879-7888.

[21] H. M.Mousa,K. H.Hussein,H. M.Woo,C. HeePark,C. SangKim, One-step anodization deposition of anticorrosive bioceramic compounds on AZ31B magnesium alloy for biomedical application, Ceram. Int. 41 (2015) 10861-10870.

[22] X. Lin, X. Wang, L. Tan, P. Wan, X. Yu, Q. Li, Effect of preparation parameters on the properties of hydroxyapatite containing micro-arc oxidation coating on biodegradable ZK60 magnesium alloy, Ceram. Int. 40 (2014) 10043-10051.

[23] T. M. Mukhametkaliyev, T.M.Mukhametkaliyev, M.A.Surmeneva, A.Vladescu, C.M.Cotrut, M.Braic, M.Dinu, M.D.Vranceanu, I.Pana, M.Mueller, R.A.Surmenev, A biodegradable AZ91 magnesium alloy coated with a thin nanostructured hydroxyapatite for improving the corrosion resistance, Mater. Sci. Eng. C. 75 (2017) 95–103.

[24] H. Hornberger, S. Virtanen, A. R. Boccaccini, Biomedical coatings on magnesium alloys - A review, Acta Biomater. 8 (2012) 2442–2455.

[25] R. B. Heimann, H. D. Lehmann, Bioceramic Coatings for Medical Implants: Trends and Techniques, Wiley-VCH Verlag GmbH & Co, Weinheim, 2015, pp. 135-263.

[26] R. B. Heimann, Thermal spraying of biomaterials, Surf. Coatings Technol. 201 (2006) 2012–2019.

[27] R. S. Pillai,M. Frasnelli,Vincenzo, M.Sglavo, HA/β-TCP plasma sprayed coatings on Ti substrate for biomedical applications, Ceram. Int. 44 (2018) 1328-1333.

[28] W. S. W. Harun, R. I. M.Asri, J. Alias, F. H. Zulkifli, K. Kadirgama, S. A. C.Ghani, J. H. M. Shariffuddin, A comprehensive review of hydroxyapatite-based coatings adhesion on metallic biomaterials, Ceram. Int. 44 (2018) 1250–1268.

[28] M. Oksa, E. Turunen, T. Suhonen, T. Varis, S.-P. Hannula, Optimization and Characterization of High Velocity Oxy-fuel Sprayed Coatings: Techniques, Materials, and Applications, Coatings. 1 (2011) 17–52.

[29] J. Fernández, M. Gaona, J. M. Guilemany, Effect of Heat Treatments on HVOF Hydroxyapatite Coatings, J. Therm. Spray Technol. 16 (2007) 220–228.

[30] S. Hasan, J. Stokes, Design of experiment analysis of the Sulzer Metco DJ high velocity oxy-fuel coating of hydroxyapatite for orthopedic applications, J. Therm. Spray Technol. 20 (2011) 186–194.

[31] R. S. Lima, K. A. Khor, H. Li, P. Cheang, B. R. Marple, HVOF spraying of nanostructured hydroxyapatite for biomedical applications, Mater. Sci. Eng. A, 396 (2005) 181–187.

[32] Gheitanchi, R., Kharaziha, M., Emadi, R., Sr-doped forsterite nanopowder: Synthesis and biological properties, Ceram. Int., 43 (2017) 12018-12025.

[33] C. Blawert, W. Dietzel, E. Ghali, G. Song, Anodizing Treatments for Magnesium Alloys and Their Effect on Corrosion Resistance in Various Environments, Adv. Eng. Mater. 8 (2006) 511–533.

[34] G. R. Argade, S. K. Panigrahi, and R. S. Mishra, Effects of grain size on the corrosion resistance of wrought magnesium alloys containing neodymium, Corros. Sci. 58 (2012) 145–151.

[35] J. Yang, X. Lu, C. Blawert, S. Di, M. L. Zheludkevich, Microstructure and corrosion behavior of Ca/P coatings prepared on magnesium by plasma electrolytic oxidation, Surf. Coatings Technol. 319 (2017) 359–369.

[36] D. Ke, S. F. Robertson, W. S. Dernell, A. Bandyopadhyay, S. Bose, Effects of MgO and SiO2 on Plasma-Sprayed Hydroxyapatite Coating: An in Vivo Study in Rat Distal Femoral Defects, ACS Appl. Mater. Interfaces. 9 (2017) 25731–25737.

[37] M. Kheirkhah, M. Fathi, H. R. Salimijazi, and M. Razavi, Surface modification of stainless steel implants using nanostructured forsterite (Mg2SiO4) coating for biomaterial applications, Surf. Coatings Technol. 276 (2015) 580–586.

Figures

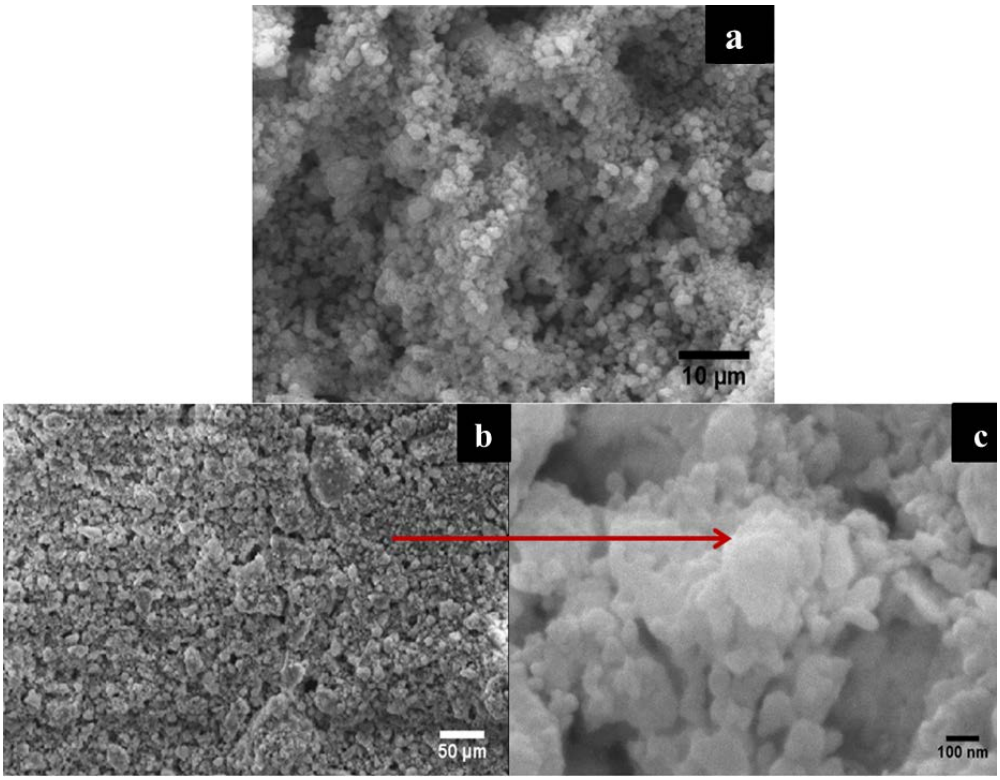

Fig.1. Morphology of (a) as synthesized and (b, c) spray dried HA powders

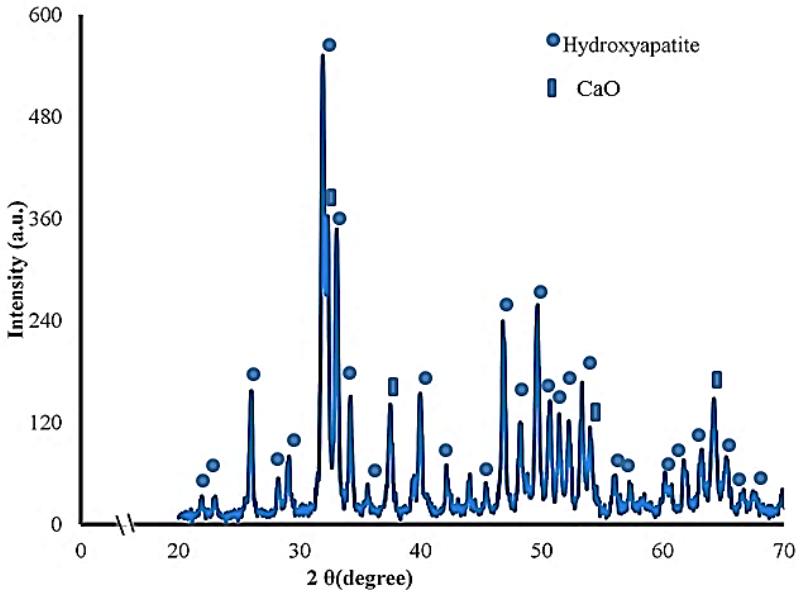

Fig.2. XRD pattern of the synthesized HA feedstock

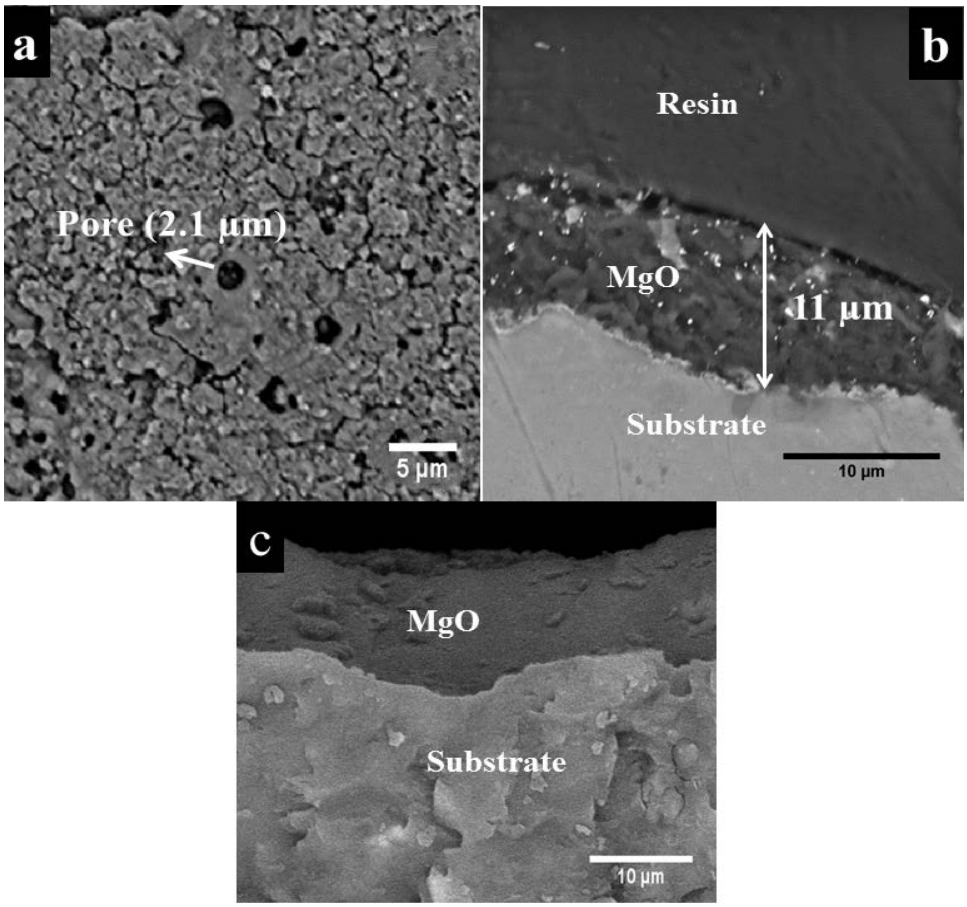

Fig.3. (a) Microstructure of the anodized layer surface, (b) Cross sectional microstructure of the anodized layer, and (c) fracture surface of the anodized layer

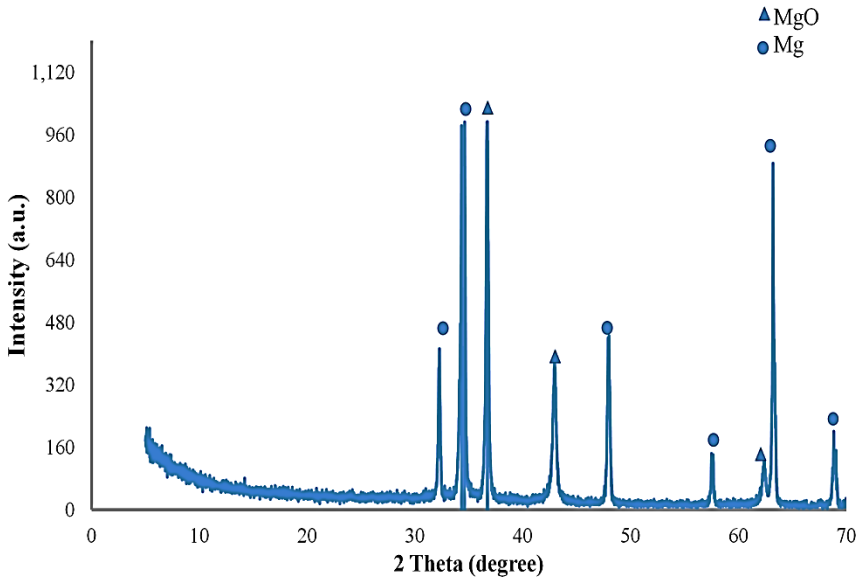

Fig.4. XRD pattern of Mg and MgO

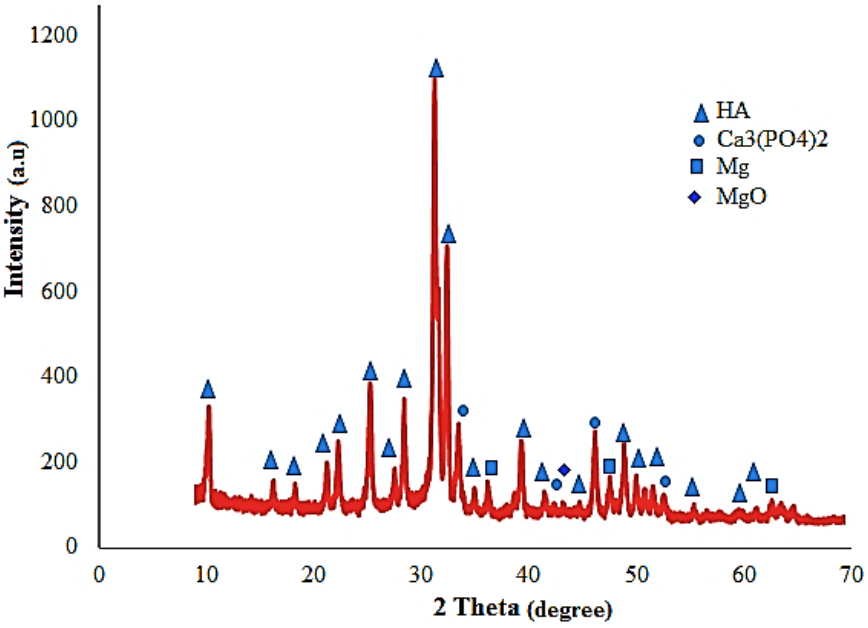

Fig.5.XRD patterns of HA coating form near surface and deeper layer

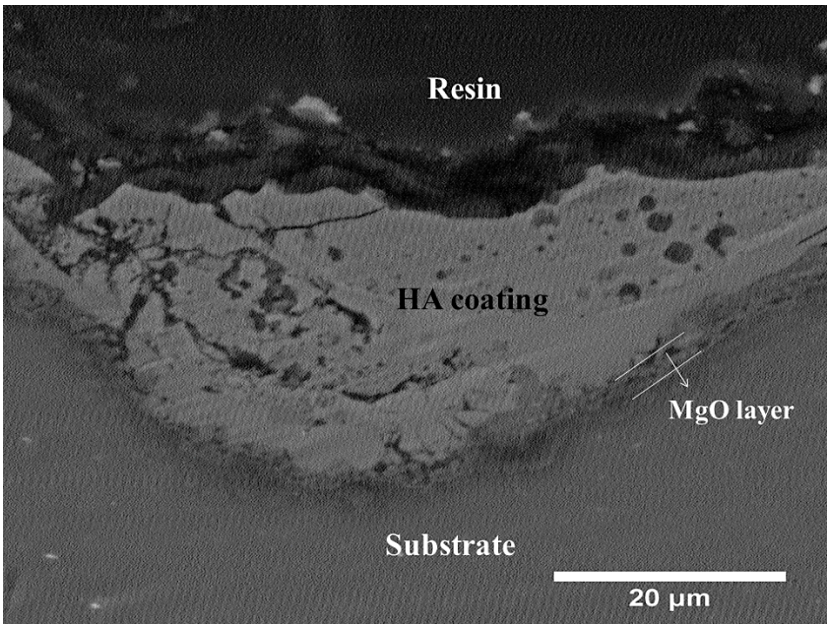

Fig.6. Cross-sectional microstructure of HA coating

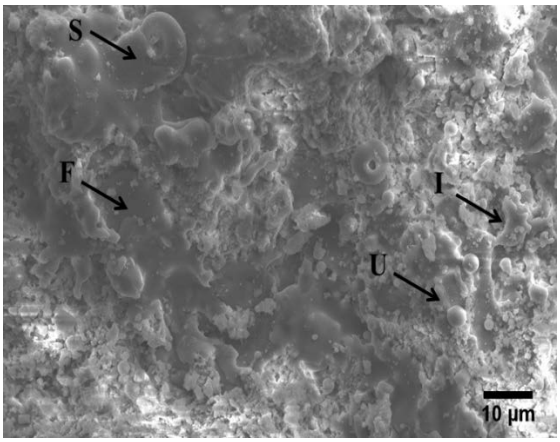

Fig.7. Surface morphology of HA coating, F = flattened splat; U = un-melted particle; S = semi-melted particles, I= inter-splat microcrack

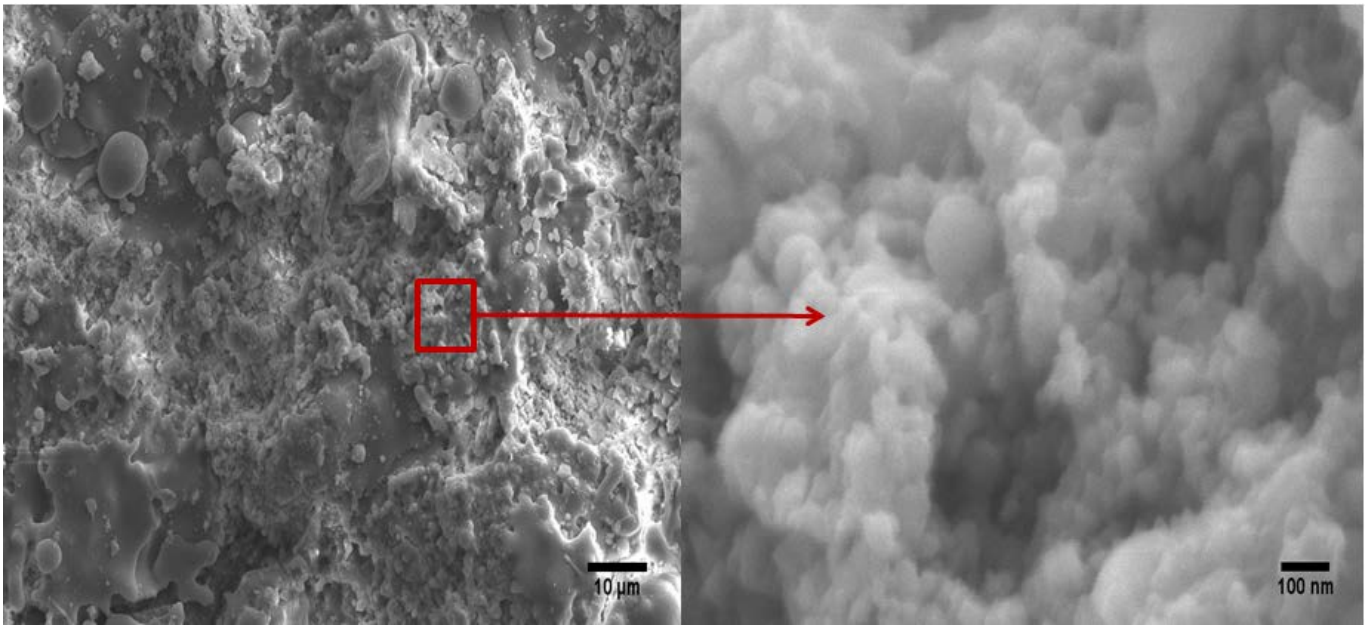

Fig.8. Microstructure of the surface of HVOF sprayed HA coating

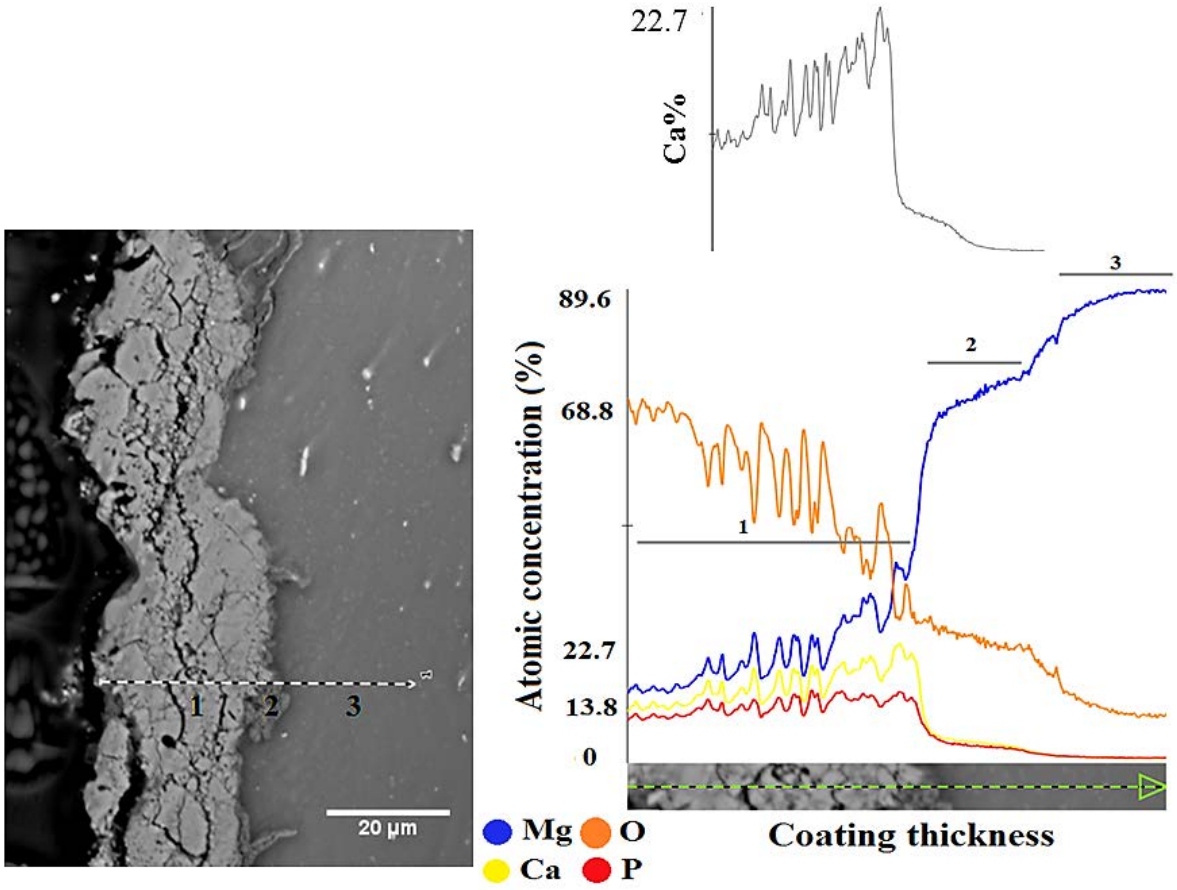

Fig.9.Elemental linear analysis from the cross section of HA coating

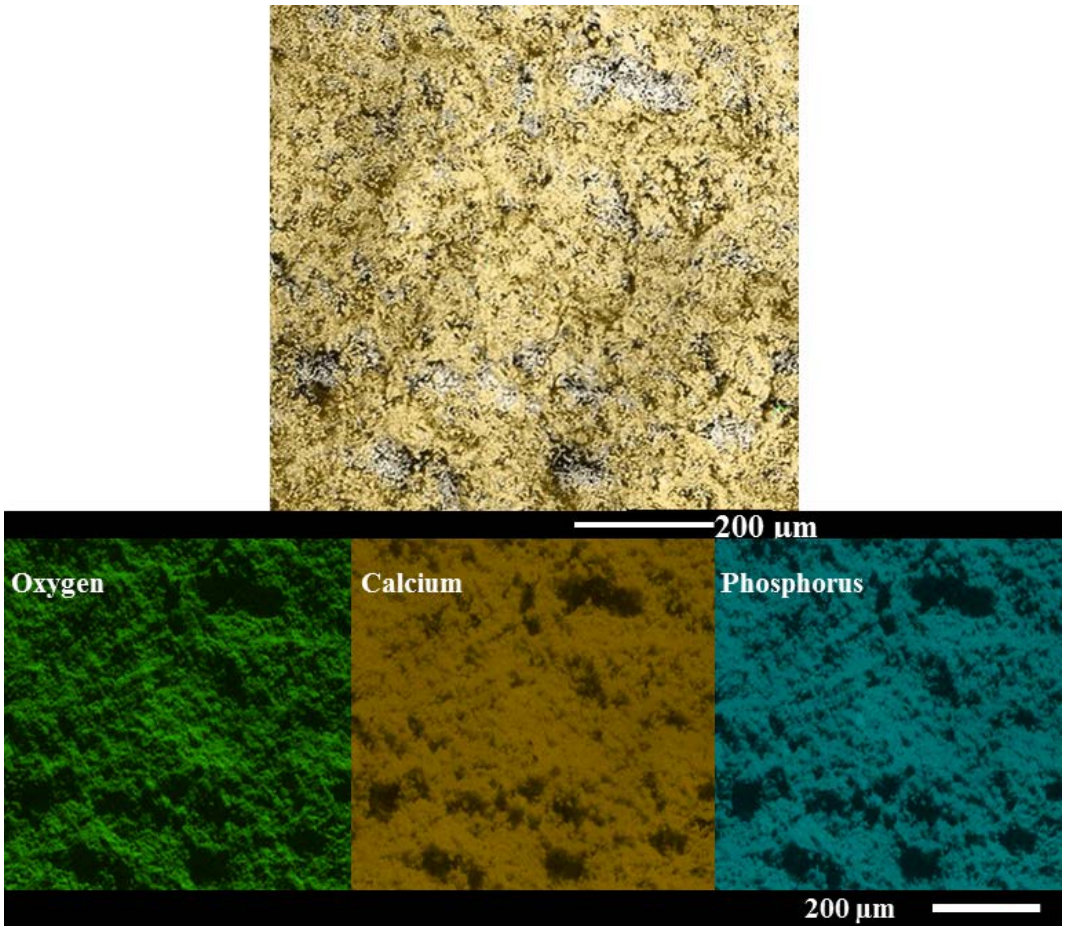

Fig.10. Elemental distribution map of HA coating surface

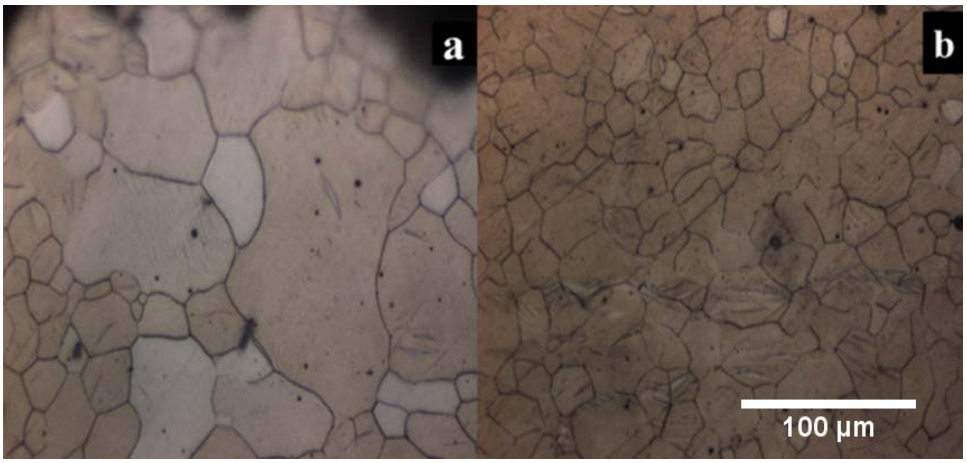

Fig.11. Optical micrographs of the substrate's cross-section. (a) near the sub surface of coating, (b) surface of deeper regions

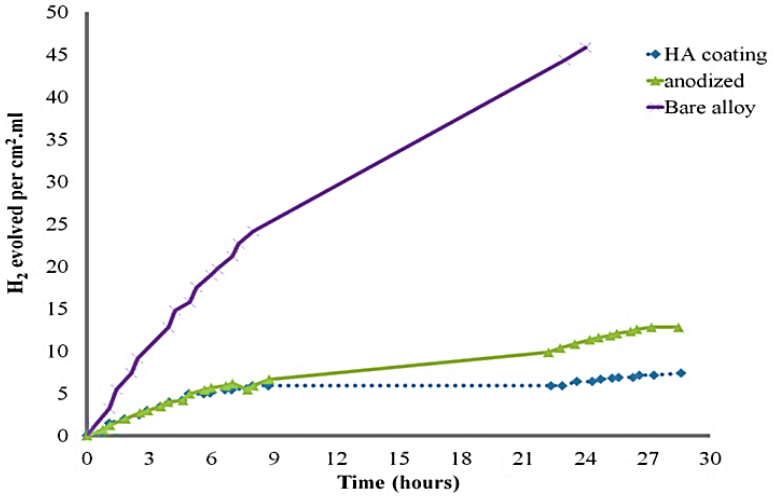

Fig.12. Normalized hydrogen evolution test during 30 hours in the SBF solution

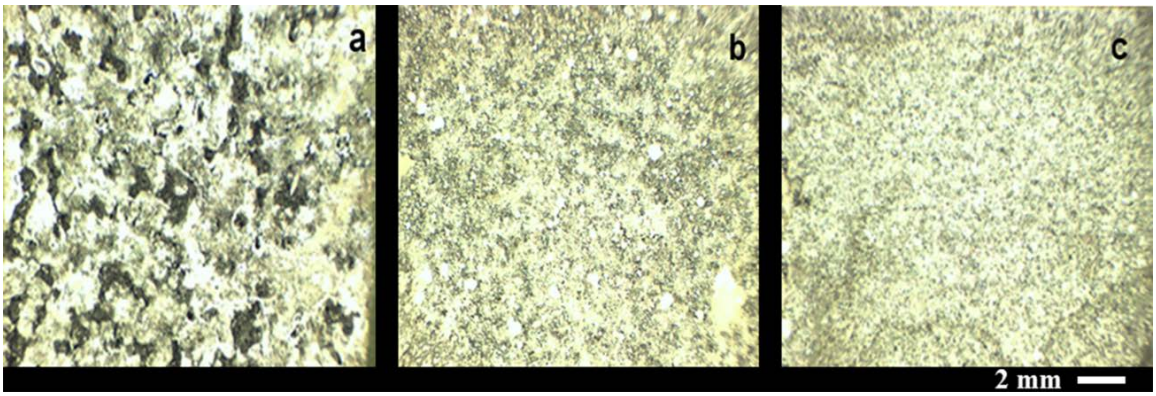

Fig.13. Surface of (a) bare alloy, (b) anodized and (c) anodized and HA coated samples after 30 hours immersion in SBF solution

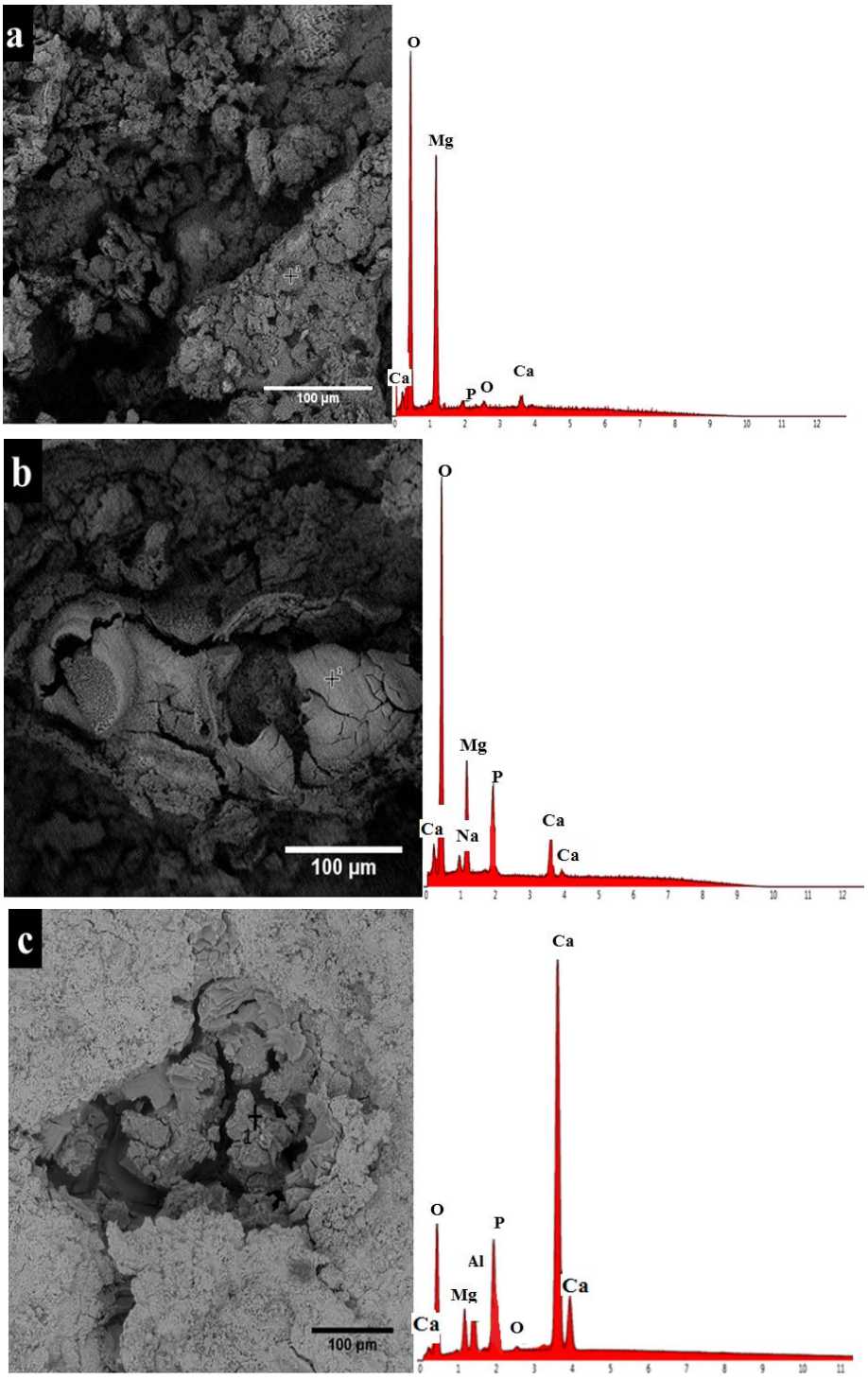

Fig.14. Morphology and analysis of the anodized and HA coated sample surface after Hydrogen evolution test

Table.1.Process parameters for HVOF process

Oxygen	Kerosene	Scan rate	Spray distance
850 L/min	24 L/h	0.5 m/sec	35 cm

Table.2. Chemical composition of SBF solution for 1000ml

Reagent	NaCl	$NaHCO_3$	KCl	$K_2HPO_4.3H_2O$	$MgCl_2.6H_2O$	1.0M-HCl	$CaCl_2$	Na_2SO_4	Tris	1.0 M-HCl
Amount	8.035g	0.355g	0.225g	0.231 g	0.311g	39ml	0.292g	0.072g	6.11g	0-5ml

Table.3. Mean chemical composition of HA coating surface by EDX analysis

	O	Ca	P
Atomic conc.	73.20	16.86	9.94

Table.4. Weight loss and corrosion rate of samples after H_2 evolution tests

	Bare	Anodized	HA coating
Weight loss (mg/cm^2)	32	6.5	6.3
Corrosion rate ($mg/cm^2.h$)	0.26	0.05	0.05

Table.5. Analysis of the anodized and HA coated samples after immersion for 30 h in SBF by EDX.

	O (wt%)	Ca (wt%)	P (wt%)	Mg (wt%)	Al (wt%)	Cl (wt%)	Na (wt%)	Ca/P
Bare alloy	73.62	1.44	0.69	23.62	-	0.54	-	2.08
Anodized	76.76	7.81	3.49	9.83	-	-	2.10	2.24
HA coating	68.27	19.03	4.91	4.01	3.60	0.18	-	3.87